Review in Advance first posted online on January 7, 2013. (Changes may still occur before final publication online and in print.)

# Ring-Polymer Molecular Dynamics: Quantum Effects in Chemical Dynamics from Classical Trajectories in an Extended Phase Space

Scott Habershon,[1] David E. Manolopoulos,[2] Thomas E. Markland,[3] and Thomas F. Miller III[4]

[1]Department of Chemistry, University of Warwick, Coventry CV4 7AL, United Kingdom; email: S.Habershon@warwick.ac.uk

[2]Physical and Theoretical Chemistry Laboratory, University of Oxford, Oxford OX1 3QZ, United Kingdom; email: david.manolopoulos@chem.ox.ac.uk

[3]Department of Chemistry, Stanford University, Stanford, California 94305; email: tmarkland@stanford.edu

[4]Department of Chemistry and Chemical Engineering, California Institute of Technology, Pasadena, California 91125; email: tfm@caltech.edu



Annu. Rev. Phys. Chem. 2013. 64:387–413

The *Annual Review of Physical Chemistry* is online at physchem.annualreviews.org

This article's doi: 10.1146/annurev-physchem-040412-110122



## Keywords

quantum dynamics, path integral, tunneling, zero-point energy, time-correlation function, semiclassical theory

## Abstract

This article reviews the ring-polymer molecular dynamics method for condensed-phase quantum dynamics. This method, which involves classical evolution in an extended ring-polymer phase space, provides a practical approach to approximating the effects of quantum fluctuations on the dynamics of condensed-phase systems. The review covers the theory, implementation, applications, and limitations of the approximation.

## 1. INTRODUCTION

Molecular dynamics (MD) simulations are among the most powerful and important tools of modern computational chemistry (1, 2). Classical MD simulations can be used to calculate a wide range of experimentally observable dynamical properties, such as diffusion coefficients, dipole absorption and neutron scattering spectra, and chemical reaction rates. However, classical MD neglects quantum mechanical zero-point energy (ZPE) and tunneling effects in the atomic motion. In systems containing light atoms at low temperatures, these effects must be included to obtain the correct quantitative, and sometimes even qualitative, behavior. For example, tunneling through the reaction barrier can easily enhance the rate of a proton or hydride transfer reaction at room temperature by several orders of magnitude.

Exact solutions of the time-dependent Schrödinger equation are in practice limited to only a few degrees of freedom or the calculation of short-timescale properties. Various approximate methods have therefore been developed for the treatment of complex, many-particle systems. Three of the most successful approaches are the linearized semiclassical initial value representation (LSC-IVR) (3–5), centroid molecular dynamics (CMD) (6, 7), and ring-polymer molecular dynamics (RPMD) (8–11). Each of these employs classical trajectories to model real-time dynamics, but in different ways. The LSC-IVR evolves purely classical trajectories from an initially quantized phase-space distribution. CMD and RPMD make use of the imaginary-time path integral formalism, which exploits the exact equilibrium mapping between a quantum mechanical particle and a classical ring polymer (12). CMD is classical MD on an effective potential generated by the thermal fluctuations of the ring polymer around its centroid, whereas RPMD is classical MD in the extended ring-polymer phase space.

Each of these methods can be used to calculate dynamical properties in quantum mechanical systems that contain hundreds, or even thousands, of atoms and for timescales that range from femtoseconds to nanoseconds. As well as relying on classical trajectories, the efficiency of these approaches for large systems arises from their neglect of real-time quantum coherence. This is an entirely reasonable approximation for many condensed-phase problems, in which thermal averaging and strong intermode coupling lead to rapid quantum decoherence (13–15).

The CMD and LSC-IVR methods were extensively reviewed several years ago (16–18). Meanwhile, applications of RPMD have grown dramatically (19–39), and intriguing connections have emerged between it and other semiclassical theories (40). It is thus timely to review the underlying theory, computational implementation, applications, and limitations of the RPMD approximation to quantum dynamics.

## 2. THEORY

### 2.1. Quantum Mechanical Correlation Functions

Many dynamical properties of systems in thermal equilibrium can be related to real-time-correlation functions of the form

$$c_{AB}(t) = \frac{1}{Q}\mathrm{tr}[e^{-\beta\hat{H}}\,\hat{A}(0)\,\hat{B}(t)], \tag{1}$$

where $Q$ is the canonical partition function,

$$Q = \mathrm{tr}[e^{-\beta\hat{H}}], \tag{2}$$

$\beta = 1/k_{\mathrm{B}}T$, and $\hat{A}(0)$ and $\hat{B}(t)$ are Heisenberg-evolved operators at times 0 and $t$:

$$\hat{O}(t) = e^{+i\hat{H}t/\hbar}\,\hat{O}\,e^{-i\hat{H}t/\hbar}. \tag{3}$$

For example, the diffusion coefficient of a molecule in a liquid can be calculated from its velocity autocorrelation function ($\hat{A} = \hat{B} = \hat{\boldsymbol{v}}$) (41); the infrared absorption spectrum of a liquid is related to its dipole autocorrelation function ($\hat{A} = \hat{B} = \hat{\boldsymbol{\mu}}$) (42); and the rate coefficient of a chemical reaction is determined by its reactive flux autocorrelation function ($\hat{A} = \hat{B} = \hat{f}$) (43), where $\hat{\boldsymbol{v}}$, $\hat{\boldsymbol{\mu}}$, and $\hat{f}$ are the operators for the velocity of the molecular center of mass, the dipole moment of the liquid, and the flux of reactants through a transition-state dividing surface, respectively.

The correlation function in Equation 1 is written in the standard way as the thermal average of the operator product $\hat{A}(0)\hat{B}(t)$. However, this is not the only possibility. A more symmetric alternative is the Kubo-transformed (44) correlation function

$$\tilde{c}_{AB}(t) = \frac{1}{\beta Q}\int_0^\beta \mathrm{tr}[e^{-(\beta-\lambda)\hat{H}}\,\hat{A}(0)e^{-\lambda\hat{H}}\,\hat{B}(t)]d\lambda, \tag{4}$$

in which the Boltzmann operator $e^{-\beta\hat{H}}$ is averaged between $\hat{A}(0)$ and $\hat{B}(t)$. This differs from $c_{AB}(t)$ because the operators $\hat{A}$ and $\hat{B}$ generally do not commute with $\hat{H}$. However, it is straightforward to show, by evaluating the traces in Equations 1 and 4 in the basis of energy eigenstates, that the Fourier transforms

$$C_{AB}(\omega) = \int_{-\infty}^{\infty} e^{-i\omega t}c_{AB}(t)dt, \quad \tilde{C}_{AB}(\omega) = \int_{-\infty}^{\infty} e^{-i\omega t}\tilde{c}_{AB}(t)dt \tag{5}$$

are related by

$$C_{AB}(\omega) = \frac{\beta\hbar\omega}{1-e^{-\beta\hbar\omega}}\tilde{C}_{AB}(\omega), \tag{6}$$

so knowledge of either of the two correlation functions is sufficient to determine the other.

The RPMD model focuses on the Kubo-transformed correlation function in Equation 4. This is the most classical form of the quantum correlation function that one can construct and therefore the best suited to a classical-like approximation. There are several reasons for this, the most fundamental being that the Kubo-transformed correlation function plays the same role in the quantum mechanical version of linear response theory as the classical correlation function plays in classical linear response theory (41). The Kubo-transformed correlation function also has the same symmetry properties as a classical correlation function (8), and the Kubo-transformed position and velocity autocorrelation functions are identical to the corresponding classical autocorrelation functions for a harmonic oscillator.

## 2.2. Ring-Polymer Molecular Dynamics

Let us consider a simple one-dimensional model system with a Hamiltonian of the form

$$\hat{H} = \frac{\hat{p}^2}{2m} + V(\hat{q}), \tag{7}$$

in which the potential energy $V(q)$ is such that the partition function in Equation 2 is well defined. The $n$-bead imaginary-time path integral (45) approximation to this partition function can then be written as (8)

$$Q_n = \frac{1}{(2\pi\hbar)^n}\int d^n\mathbf{p}\int d^n\mathbf{q}\, e^{-\beta_n H_n(\mathbf{p},\mathbf{q})}, \tag{8}$$

where $H_n(\mathbf{p},\mathbf{q})$ is the classical Hamiltonian of a ring polymer consisting of $n$ copies of the system connected by harmonic springs (12)

$$H_n(\mathbf{p},\mathbf{q}) = \sum_{j=1}^{n}\left[\frac{p_j^2}{2m} + \frac{1}{2}m\omega_n^2(q_j - q_{j-1})^2 + V(q_j)\right], \tag{9}$$

with $\beta_n = \beta/n$, $\omega_n = 1/(\beta_n\hbar)$, and $q_0 \equiv q_n$. This is the basis of the path integral molecular dynamics (PIMD) method (46), which uses the classical dynamics generated by the Hamiltonian in Equation 9,

$$\dot{\mathbf{p}} = -\frac{\partial H_n(\mathbf{p},\mathbf{q})}{\partial \mathbf{q}}, \quad \dot{\mathbf{q}} = +\frac{\partial H_n(\mathbf{p},\mathbf{q})}{\partial \mathbf{p}}, \tag{10}$$

as a sampling device to explore the configuration space of the ring polymer and calculate the exact thermodynamic and structural properties of the system in the limit of a sufficiently large number of beads.

The RPMD model uses the same trajectories to provide a classical-like approximation to Kubo-transformed quantum correlation functions of the form in Equation 4. For the case in which the correlated operators $\hat{A}$ and $\hat{B}$ are local (functions of the coordinate operator $\hat{q}$), this RPMD approximation is simply (8)

$$\tilde{c}_{AB}(t) \simeq \frac{1}{(2\pi\hbar)^n Q_n} \int d^n\mathbf{p}_0 \int d^n\mathbf{q}_0 e^{-\beta_n H_n(\mathbf{p}_0,\mathbf{q}_0)} A_n(\mathbf{q}_0) B_n(\mathbf{q}_t), \tag{11}$$

where the functions $A_n(\mathbf{q}_0)$ and $B_n(\mathbf{q}_t)$ are averaged over the beads of the ring-polymer necklace at times 0 and $t$:

$$A_n(\mathbf{q}) = \frac{1}{n}\sum_{j=1}^{n} A(q_j), \quad B_n(\mathbf{q}) = \frac{1}{n}\sum_{j=1}^{n} B(q_j). \tag{12}$$

We note that the correlation function in Equation 11 is just a classical correlation function in the extended phase space of the $n$-bead imaginary-time path integral. This is the central feature of RPMD.

We do not yet know how to provide a systematic derivation of the approximation in Equation 11. However, we note that the classical trajectories of the ring-polymer necklace have long been recognized to offer insight into the relaxation of a quantum system in real time (46–48). Furthermore, we can at least motivate the RPMD approximation by showing that it gives the exact quantum mechanical result in various limiting cases. These include the following.

**2.2.1. High-temperature limit.** In the high-temperature limit, the harmonic spring force constant $m\omega_n^2$ in Equation 9 becomes so large that the radius of gyration of the ring polymer shrinks to zero. Under these circumstances, it suffices to use just a single bead ($n = 1$), in which case Equation 8 reduces to the classical partition function and Equation 11 to the classical correlation function. These are the correct quantum mechanical results in the regime where $\beta\hbar\omega_{\max} \ll 1$, where $\omega_{\max}$ is the highest vibrational frequency in the physical problem.

**2.2.2. Short-time limit.** The ring-polymer correlation function in Equation 11 coincides with the exact Kubo-transformed quantum mechanical correlation function in Equation 4 in the limit as $t \to 0$ (8). To see this in detail, one can expand the correlation functions in the two equations in Taylor series around $t = 0$, considering for simplicity the case in which $A(\hat{q})$ and $B(\hat{q})$ are Hermitian operators (11). Only the even expansion coefficients survive in this case because the exact $\tilde{c}_{AB}(t)$ and its RPMD approximation are both real and even functions of $t$ (8). Comparison of the exact and approximate expansion coefficients reveals that the RPMD approximation has a leading error of $O(t^8)$ for the position autocorrelation function and an error of $O(t^4)$ for a more general correlation function involving nonlinear operators $A(\hat{q})$ and $B(\hat{q})$ (11).

**2.2.3. Harmonic oscillator limit.** When the potential $V(q)$ is that of a simple harmonic oscillator, it is straightforward to show (8) that Equation 11 will give the exact quantum mechanical result

(in the limit as $n \to \infty$) for all correlation functions of the form $\tilde{c}_{Aq}(t)$ and $\tilde{c}_{qB}(t)$. The position autocorrelation function $\tilde{c}_{qq}(t)$ of a harmonic oscillator is a special case in which the exact result is obtained with any value of $n$ (8).

**2.2.4. Static equilibrium limit.** When the operator $\hat{A}$ is the unit operator ($\hat{A} = \hat{1}$), one can cyclically permute the order of the operators in the trace in Equation 4 and exploit the commutativity of the Boltzmann operator $e^{-\beta \hat{H}}$ with the real-time evolution operators $e^{\pm i \hat{H} t/\hbar}$ to show that $\tilde{c}_{AB}(t)$ reduces to the static thermal expectation value of the operator $\hat{B}$:

$$\tilde{c}_{1B}(t) = \frac{1}{Q} \mathrm{tr}[e^{-\beta \hat{H}} \hat{B}] \equiv \langle B \rangle. \tag{13}$$

It is therefore interesting to consider what happens in Equation 11 when $A_n(\mathbf{q}_0) = 1$. Because the classical ring-polymer dynamics in Equation 10 conserves both the Boltzmann factor

$$e^{-\beta_n H_n(\mathbf{p}_0, \mathbf{q}_0)} = e^{-\beta_n H_n(\mathbf{p}_t, \mathbf{q}_t)} \tag{14}$$

and the phase-space volume element

$$d^n \mathbf{p}_0 d^n \mathbf{q}_0 = d^n \mathbf{p}_t d^n \mathbf{q}_t, \tag{15}$$

we have

$$\tilde{c}_{1B}(t) \simeq \frac{1}{(2\pi\hbar)^n Q_n} \int d^n \mathbf{p}_t \int d^n \mathbf{q}_t e^{-\beta_n H_n(\mathbf{p}_t, \mathbf{q}_t)} B_n(\mathbf{q}_t). \tag{16}$$

Relabeling $\mathbf{p}_t$ and $\mathbf{q}_t$ as $\mathbf{p}$ and $\mathbf{q}$, one sees that this is just the $n$-bead path integral expression for $\langle B \rangle$. The RPMD approximation therefore becomes exact for $\hat{A} = \hat{1}$ in the limit as $n \to \infty$.

The last of these limiting cases is especially important for applications of the RPMD model to condensed-phase systems because it confirms that the (fictitious) classical dynamics of the ring polymers is at least consistent with the quantum mechanical equilibrium distribution, as one would expect from the connection between RPMD and PIMD. This implies, among other things, that an RPMD simulation at a given *NVT* thermodynamic state point will sample the correct quantum mechanical configurational distribution (19) and that initially quantized ZPE will not flow unphysically from the high-frequency intramolecular modes to the low-frequency intermolecular modes during an RPMD simulation of a molecular liquid (29).

## 2.3. Nonlocal Operators

So far, we have only considered correlation functions involving local operators $A(\hat{q})$ and $B(\hat{q})$. However, the vast majority of correlation functions of interest in applications involve either local operators or their (Heisenberg) time derivatives, and correlation functions involving the time derivatives of local operators are also amenable to calculation within the RPMD approximation.

For example, the fact that the velocity operator is the Heisenberg time derivative of the position operator,

$$\hat{v} = \frac{i}{\hbar}[\hat{H}, \hat{q}], \tag{17}$$

can be used to show that the exact quantum mechanical Kubo-transformed velocity autocorrelation function,

$$\tilde{c}_{vv}(t) = \frac{1}{\beta Q} \int_0^\beta \mathrm{tr}[e^{-(\beta-\lambda)\hat{H}} \hat{v}(0) e^{-\lambda \hat{H}} \hat{v}(t)] d\lambda, \tag{18}$$

is related to the position autocorrelation function,

$$\tilde{c}_{qq}(t) = \frac{1}{\beta Q}\int_0^\beta \mathrm{tr}[e^{-(\beta-\lambda)\hat{H}}\,\hat{q}(0)e^{-\lambda\hat{H}}\,\hat{q}(t)]d\lambda, \tag{19}$$

by

$$\tilde{c}_{vv}(t) = -\frac{d^2}{dt^2}\tilde{c}_{qq}(t). \tag{20}$$

To develop an RPMD approximation to $\tilde{c}_{vv}(t)$, we can therefore simply write down the approximation to $\tilde{c}_{qq}(t)$,

$$\tilde{c}_{qq}(t) \simeq \frac{1}{(2\pi\hbar)^n Q_n}\int d^n\mathbf{p}_0 \int d^n\mathbf{q}_0 e^{-\beta_n H_n(\mathbf{p}_0,\mathbf{q}_0)}\bar{q}_0\bar{q}_t, \tag{21}$$

where

$$\bar{q} = \frac{1}{n}\sum_{j=1}^n q_j, \tag{22}$$

and differentiate (minus) this twice with respect to $t$. Exploiting again the conservation of the ring-polymer Boltzmann factor in Equation 14 and the phase-space volume element in Equation 15, one finds that the result of this differentiation can be written in the form (19)

$$\tilde{c}_{vv}(t) \simeq \frac{1}{(2\pi\hbar)^n Q_n}\int d^n\mathbf{p}_0 \int d^n\mathbf{q}_0 e^{-\beta_n H_n(\mathbf{p}_0,\mathbf{q}_0)}\bar{v}_0\bar{v}_t, \tag{23}$$

where

$$\bar{v} = \frac{1}{nm}\sum_{j=1}^n p_j. \tag{24}$$

The RPMD approximation to the Kubo-transformed velocity autocorrelation function therefore emerges in an entirely natural way as involving the correlation between the velocities of the ring-polymer centroids at times 0 and $t$.

## 2.4. Ring-Polymer Rate Theory

The simplest model for a bimolecular chemical reaction is a one-dimensional barrier transmission problem in which the potential energy $V(q)$ tends toward zero as $q \to -\infty$ (the reactant asymptote) and to a constant as $q \to \infty$ (the product asymptote), with a reaction barrier somewhere in between.

According to Miller et al. (43), the exact quantum mechanical thermal rate coefficient for this reaction can be written as

$$k(T) = \frac{1}{Q_r(T)}\lim_{t\to\infty}\tilde{c}_{fs}(t) = \frac{1}{Q_r(T)}\int_0^\infty \tilde{c}_{ff}(t)dt, \tag{25}$$

where $Q_r(T) = (m/2\pi\beta\hbar^2)^{1/2}$ is the reactant partition function per unit length (it would become the reactant partition function per unit volume for a reaction in three-dimensional space), and $\tilde{c}_{fs}(t)$ and $\tilde{c}_{ff}(t)$ are the (Kubo-transformed) flux-side and flux-flux correlation functions,

$$\tilde{c}_{fs}(t) = \frac{1}{\beta}\int_0^\beta \mathrm{tr}[e^{-(\beta-\lambda)\hat{H}}\,\hat{f}(0)e^{-\lambda\hat{H}}\,\hat{h}(t)]d\lambda \tag{26}$$

and

$$\tilde{c}_{ff}(t) = \frac{1}{\beta}\int_0^\beta \mathrm{tr}[e^{-(\beta-\lambda)\hat{H}}\,\hat{f}(0)e^{-\lambda\hat{H}}\,\hat{f}(t)]d\lambda. \tag{27}$$

Here

$$\hat{h} = h(\hat{q} - q^{\ddagger}) \tag{28}$$

is a local (configurational) Heaviside operator that projects onto states on the product side of a transition-state dividing surface at $s(q) = q - q^{\ddagger} = 0$, and

$$\hat{f} = \frac{i}{\hbar}[\hat{H}, \hat{h}] \tag{29}$$

is its Heisenberg time derivative—the operator for the flux of reactants through the dividing surface.

Because the flux operator is the time derivative of the side operator, and the side operator is a local operator, one can develop an RPMD approximation to the flux-side correlation function in Equation 26 by first writing down the RPMD expression for (minus) the side-side correlation function and then differentiating this once with respect to $t$ (9). However, the resulting expression is not in the most useful form. It is possible to obtain a more convenient expression in which the correlation is transferred from an average over the ring-polymer beads to the ring-polymer centroid by noting that the rate coefficient depends only on the value of $\tilde{c}_{fs}(t)$ in the limit as $t \to \infty$ (10). The final result is the rate coefficient

$$k^{\mathrm{RPMD}}(T) = \frac{1}{Q_r(T)} \lim_{t\to\infty} \bar{c}_{fs}(t), \tag{30}$$

where

$$\bar{c}_{fs}(t) = \frac{1}{(2\pi\hbar)^n} \int d^n\mathbf{p}_0 \int d^n\mathbf{q}_0 e^{-\beta_n H_n(\mathbf{p}_0,\mathbf{q}_0)} \bar{v}_0 \delta(\bar{q}_0 - q^{\ddagger}) h(\bar{q}_t - q^{\ddagger}), \tag{31}$$

with $\bar{q}$ and $\bar{v}$ as defined in Equations 22 and 24.

This is again simply a classical expression in the extended phase space of the ring polymer, and it again has a number of appealing features. These include the following.

**2.4.1. High-temperature (classical) limit.** In the high-temperature limit, in which the ring polymer shrinks to a single bead ($n = 1$), Equation 31 becomes the classical flux-side correlation function, and $k^{\mathrm{RPMD}}(T)$ becomes the classical rate coefficient. This coincides with the exact quantum mechanical rate coefficient in the high-temperature limit.

**2.4.2. Short-time (transition-state-theory) limit.** The short-time limit of the RPMD flux-side correlation function in Equation 31 is especially interesting. As $t \to 0_+$, the step function in the displacement from the dividing surface $h(\bar{q}_t - q^{\ddagger})$ can be replaced with a step function in the initial velocity $h(\bar{v}_0)$, and a straightforward calculation then shows that

$$\frac{1}{Q_r(T)} \lim_{t\to 0_+} \bar{c}_{fs}(t) = \frac{1}{2}\langle|v|\rangle_{\mathrm{cl}} \frac{Q(q^{\ddagger})}{Q_r(T)}, \tag{32}$$

where the first factor is the (purely classical) thermal expectation value of $\bar{v}_0 h(\bar{v}_0)$,

$$\frac{1}{2}\langle|v|\rangle_{\mathrm{cl}} = \left(\frac{1}{2\pi\beta m}\right)^{1/2}, \tag{33}$$

and $Q(q^{\ddagger})$ is the centroid-constrained partition function

$$Q(q^{\ddagger}) = \frac{1}{(2\pi\hbar)^n} \int d^n\mathbf{p}_0 \int d^n\mathbf{q}_0 e^{-\beta_n H_n(\mathbf{p}_0,\mathbf{q}_0)} \delta(\bar{q}_0 - q^{\ddagger}). \tag{34}$$

The right-hand side of Equation 32 is the well-known centroid density (49, 50) quantum transition-state theory (QTST) approximation to the rate coefficient (51), which therefore emerges automatically from the short-time limit of RPMD rate theory.

It follows that the RPMD rate coefficient can be written equivalently as

$$k^{\mathrm{RPMD}}(T) = \lim_{t\to\infty} \kappa(t)\, k^{\mathrm{QTST}}(T), \tag{35}$$

where

$$\kappa(t) = \frac{\bar{c}_{fs}(t)}{\bar{c}_{fs}(t \to 0_+)} \tag{36}$$

is a dynamical (time-dependent) transmission coefficient. This transmission coefficient allows for recrossing of the transition-state dividing surface at $q = q^{\ddagger}$ and ensures that $k^{\mathrm{RPMD}}(T)$ will be independent of the choice of this dividing surface (10). As in the classical case, one can show that $\kappa(t) \leq 1$, so the QTST rate coefficient provides an upper bound on the RPMD rate coefficient. In effect, RPMD rate theory is to QTST what the fully dynamical classical rate theory is to classical transition-state theory.

**2.4.3. Parabolic barrier (shallow-tunneling) limit.** When the potential $V(q)$ is that of a parabolic barrier, $V(q) = -\frac{1}{2}m\omega_b^2 q^2$, an exact quantum mechanical calculation gives

$$Q_r(T)k(T) = \lim_{t\to\infty} \tilde{c}_{fs}(t) = \frac{k_{\mathrm{B}}T}{h}\frac{\beta\hbar\omega_b/2}{\sin(\beta\hbar\omega_b/2)}. \tag{37}$$

RPMD rate theory has been shown to reproduce this exact result in the limit as $n \to \infty$ (9), and it therefore correctly captures the shallow tunneling through a parabolic barrier.

**2.4.4. Low-temperature (deep-tunneling) limit.** More importantly, Richardson & Althorpe (40) have recently shown that the RPMD rate coefficient is also expected to be accurate in the deep quantum tunneling regime, where the parabolic approximation to the reaction barrier becomes irrelevant.

The onset of this deep tunneling regime is at the critical reciprocal temperature $\beta_c = 2\pi/\hbar\omega_b$ (critical temperature $T_c = \hbar\omega_b/2\pi k_{\mathrm{B}}$), at which the right-hand side of Equation 37 diverges. Below this crossover temperature, a highly accurate semiclassical description of the tunneling exists in terms of instantons—periodic orbits in imaginary time with period $\beta\hbar$ (52). A finite-difference approximation to the instanton trajectory appears as a saddle point on the ring-polymer potential energy surface (40), and Richardson & Althorpe were able to use this fact to establish a connection between [the uniform, Im F version (53, 54) of] instanton theory and ring-polymer rate theory. It follows from their analysis of this connection that RPMD will generally underestimate the rate of a reaction with a symmetric barrier and overestimate the rate of a reaction with an asymmetric barrier in the deep quantum tunneling regime. However, the underestimation and overestimation are only slight: In the temperature range between $T_c$ and $T_c/2$, in which the purely classical rate coefficient is typically in error by several orders of magnitude, the error in the RPMD rate coefficient is expected to be less than a factor of 2 (40). These theoretical predictions have since been confirmed in numerous low-dimensional reaction-rate calculations for which exact quantum mechanical results are available for comparison (27, 33, 37).

## 2.5. Multidimensional Generalization

All the equations given above are for a one-dimensional system with a Hamiltonian of the form in Equation 7. However, the great strength of (imaginary-time) path integrals is that they are

straightforward to generalize to systems with more degrees of freedom, especially when the temperature is sufficiently high that identical atom exchange effects can be ignored (as is certainly the case in most condensed-phase systems, ranging from liquid water at room temperature to liquid *para*-hydrogen at 14 K).

The generic multidimensional problem involves a system containing $N$ atoms with a Hamiltonian of the form

$$\hat{H} = \sum_{i=1}^{N} \frac{|\hat{\boldsymbol{p}}_i|^2}{2m_i} + V(\hat{\boldsymbol{q}}_1, \ldots, \hat{\boldsymbol{q}}_N), \tag{38}$$

where $\hat{\boldsymbol{p}}_i$ and $\hat{\boldsymbol{q}}_i$ are the three-dimensional momentum and position operators of atom $i$. Assuming that the atoms can be regarded as distinguishable, the $n$-bead path integral expression for the partition function of this system has exactly the same form as Equation 8,

$$Q_n = \frac{1}{(2\pi\hbar)^f} \int d^f\mathbf{p} \int d^f\mathbf{q} e^{-\beta_n H_n(\mathbf{p},\mathbf{q})}, \tag{39}$$

where $f = 3Nn$ is the total number of Cartesian degrees of freedom, and

$$H_n(\mathbf{p},\mathbf{q}) = H_n^0(\mathbf{p},\mathbf{q}) + \sum_{j=1}^{n} V(q_{1,j}, \ldots, q_{N,j}), \tag{40}$$

with

$$H_n^0(\mathbf{p},\mathbf{q}) = \sum_{i=1}^{N}\sum_{j=1}^{n}\left[\frac{|\boldsymbol{p}_{i,j}|^2}{2m_i} + \frac{1}{2}m_i\omega_n^2|\boldsymbol{q}_{i,j} - \boldsymbol{q}_{i,j-1}|^2\right], \tag{41}$$

is the appropriate multidimensional generalization of the ring-polymer Hamiltonian in Equation 9. Just as in the one-dimensional case, this is the classical Hamiltonian of an extended system containing $n$ copies of the original system, with (the same atoms in) neighboring copies connected by harmonic springs.

Given these definitions, all the other aspects of RPMD (and indeed PIMD) carry over to the multidimensional case in a straightforward way. For example, Equation 23 generalizes to give the RPMD approximation to the Kubo-transformed velocity autocorrelation function of a tagged atom $i$ in a liquid as (19)

$$\tilde{c}_{\boldsymbol{v}\cdot\boldsymbol{v}}(t) \simeq \frac{1}{(2\pi\hbar)^f Q_n} \int d^f\mathbf{p}_0 \int d^f\mathbf{q}_0 e^{-\beta_n H_n(\mathbf{p}_0,\mathbf{q}_0)} \bar{\boldsymbol{v}}_0 \cdot \bar{\boldsymbol{v}}_t, \tag{42}$$

where

$$\bar{\boldsymbol{v}} = \frac{1}{nm_i}\sum_{j=1}^{n} \boldsymbol{p}_{i,j}, \tag{43}$$

and Equation 31 generalizes to give the RPMD approximation to the flux-side correlation function of a chemical reaction as (10, 40)

$$\tilde{c}_{fs}(t) = \frac{1}{(2\pi\hbar)^f} \int d^f\mathbf{p}_0 \int d^f\mathbf{q}_0 e^{-\beta_n H_n(\mathbf{p}_0,\mathbf{q}_0)} v_s(\mathbf{p}_0,\mathbf{q}_0)\delta[s(\mathbf{q}_0)]h[s(\mathbf{q}_t)], \tag{44}$$

where the (multidimensional) dividing surface between reactants and products in ring-polymer coordinate space has been written here as $s(\mathbf{q}) = 0$, and the initial velocity factor $v_s(\mathbf{p}_0,\mathbf{q}_0)$ in Equation 44 is therefore

$$v_s(\mathbf{p},\mathbf{q}) = \sum_{i=1}^{N}\sum_{j=1}^{n} \frac{\partial s(\mathbf{q})}{\partial q_{i,j}} \cdot \frac{p_{i,j}}{m_i}. \tag{45}$$

## 3. IMPLEMENTATION

### 3.1. Preliminary Observations

Because RPMD is simply classical MD in an extended phase space, its implementation can borrow from the wealth of techniques that have been developed for performing classical MD simulations (1, 2). However, there are two special features of the RPMD equations of motion to keep in mind when implementing the method, both of which stem from the presence of the harmonic spring terms in the free ring-polymer Hamiltonian in Equation 41.

Because $\omega_n = n/(\beta\hbar)$, these springs can become very stiff in simulations that require a large number of beads. As a result of this stiffness, the classical dynamics generated by the ring-polymer Hamiltonian will almost certainly not be ergodic (55), so even a very long *NVE* trajectory will not explore the full microcanonical phase space. One way around this difficulty is to accumulate the RPMD correlation function by time averaging along a number of shorter *NVE* trajectories whose initial conditions (ring-polymer coordinates and momenta) are taken from uncorrelated snapshots of a thermostatted (*NVT*) PIMD simulation (56). This has the dual effect of correctly sampling the Boltzmann weight in the correlation function and ensuring that each new *NVE* trajectory explores a different region of microcanonical phase space. Some simple but effective stochastic thermostats for the initial PIMD stage of this calculation are described in Reference 57.

Another consequence of the stiff spring terms in the ring-polymer Hamiltonian is that the internal modes of the ring polymer vibrate rapidly. In a problem in which the highest physical frequency is $\omega_{\max}$, the fastest ring-polymer mode vibrates at a frequency as high as $\Omega_{\max} = \sqrt{\omega_{\max}^2 + (2n/\beta\hbar)^2}$. Because the path integral only begins to converge once $n > \beta\hbar\omega_{\max}$, it will certainly be true that $\Omega_{\max} > \sqrt{5}\omega_{\max}$, and $\Omega_{\max}$ will typically be several times larger than this in a fully converged calculation. It follows that if one were to use the standard velocity Verlet method (2) to integrate the ring-polymer equations of motion, it would be necessary to employ a significantly smaller time step than in a classical MD simulation. However, this difficulty can largely be eliminated by replacing the free particle evolution step of the velocity Verlet method with an exact evolution under the influence of the free ring-polymer Hamiltonian in Equation 41. With this modification, the rapid vibrations of the internal modes of the ring polymer are followed more accurately, and one can typically get away with a time step that is similar to the one employed in classical MD. The implementation of this modified velocity Verlet method is also described in Reference 57.

### 3.2. Ring-Polymer Contraction

Once the above considerations have been taken into account, one is still left with the seemingly inescapable fact that an RPMD simulation will be $n$ times more expensive than a classical simulation, owing to the need to evaluate the forces associated with the potential

$$V_n(\mathbf{q}) = \sum_{j=1}^{n} V(\boldsymbol{q}_{1,j}, \ldots, \boldsymbol{q}_{N,j}) \tag{46}$$

in Equation 40. Remarkably, even this computational overhead can largely be eliminated, at least in simulations with empirical force fields, with the help of some recently developed ring-polymer contraction techniques (58–60).

These techniques are based on the observation that the physical potential acting on each bead of the ring-polymer necklace, $V(\boldsymbol{q}_1, \ldots, \boldsymbol{q}_N)$, can typically be decomposed into a sum of a rapidly varying short-range contribution, $V_S(\boldsymbol{q}_1, \ldots, \boldsymbol{q}_N)$, and a slowly varying long-range contribution, $V_L(\boldsymbol{q}_1, \ldots, \boldsymbol{q}_N)$. For example, the part of $V(\boldsymbol{q}_1, \ldots, \boldsymbol{q}_N)$ that arises from coulomb interactions

between partial charge sites in different molecules,

$$V(\boldsymbol{q}_1, \ldots, \boldsymbol{q}_N) = \sum_{i=1}^{N} \sum_{i'>i}^{N} \frac{z_i z_{i'}}{4\pi\varepsilon_0 |\boldsymbol{q}_i - \boldsymbol{q}_{i'}|}, \tag{47}$$

can be decomposed into a short-range contribution,

$$V_S(\boldsymbol{q}_1, \ldots, \boldsymbol{q}_N) = \sum_{i=1}^{N} \sum_{i'>i}^{N} \frac{z_i z_{i'}}{4\pi\varepsilon_0 |\boldsymbol{q}_i - \boldsymbol{q}_{i'}|} [1 - f(|\boldsymbol{q}_i - \boldsymbol{q}_{i'}|)], \tag{48}$$

and a long-range contribution,

$$V_L(\boldsymbol{q}_1, \ldots, \boldsymbol{q}_N) = \sum_{i=1}^{N} \sum_{i'>i}^{N} \frac{z_i z_{i'}}{4\pi\varepsilon_0 |\boldsymbol{q}_i - \boldsymbol{q}_{i'}|} f(|\boldsymbol{q}_i - \boldsymbol{q}_{i'}|), \tag{49}$$

where the switching function

$$f(r) = \begin{cases} 2(r/\sigma) - 2(r/\sigma)^3 + (r/\sigma)^4, & r \le \sigma \\ 1, & r \ge \sigma \end{cases} \tag{50}$$

ensures that (*a*) the interactions in $V_S(\boldsymbol{q}_1, \ldots, \boldsymbol{q}_N)$ vanish continuously at $r = \sigma$ and (*b*) the interactions in $V_L(\boldsymbol{q}_1, \ldots, \boldsymbol{q}_N)$ can be made arbitrarily slowly varying by increasing $\sigma$.

Once the interactions in $V_L(\boldsymbol{q}_1, \ldots, \boldsymbol{q}_N)$ are sufficiently slowly varying over the length scale of the ring polymer (which can be estimated from the free-particle radius of gyration $\sqrt{\beta\hbar^2/4m_i}$, where $m_i$ is the mass of the lightest atom in the system), it ceases to be necessary to evaluate this part of the potential on each bead: It can be evaluated instead on a contracted ring polymer with fewer than the full $n$ beads (58). In the extreme case in which the ring polymer is contracted all the way to its centroid, this boils down to approximating $V_n(\mathbf{q})$ in Equation 46 by (59)

$$V_n(\mathbf{q}) \simeq \sum_{j=1}^{n} V_S(\boldsymbol{q}_{1,j}, \ldots, \boldsymbol{q}_{N,j}) + nV_L(\bar{\boldsymbol{q}}_1, \ldots, \bar{\boldsymbol{q}}_N), \tag{51}$$

or equivalently

$$V_n(\mathbf{q}) \simeq \sum_{j=1}^{n} [V_S(\boldsymbol{q}_{1,j}, \ldots, \boldsymbol{q}_{N,j}) - V_S(\bar{q}_1, \ldots, \bar{\boldsymbol{q}}_N)] + nV(\bar{\boldsymbol{q}}_1, \ldots, \bar{\boldsymbol{q}}_N), \tag{52}$$

where

$$\bar{\boldsymbol{q}}_i = \frac{1}{n} \sum_{j=1}^{n} \boldsymbol{q}_{i,j}. \tag{53}$$

The computational advantage of this approximation is clear from Equation 52. The full potential $V(\boldsymbol{q}_1, \ldots, \boldsymbol{q}_N)$ is evaluated just once on the ring-polymer centroid, with the same effort as in a classical MD simulation, leaving a comparatively inexpensive short-range correction to be applied to each bead. Note also that this is the only approximation one has to make: The forces that enter the ring-polymer equations of motion then follow directly from the chain rule and yield a dynamics that exactly conserves the approximate ring-polymer Hamiltonian in which $V_n(\mathbf{q})$ is replaced by the right-hand side of Equation 52.

When this procedure is applied to an empirical water model, one finds that evaluating the coulomb interactions beyond $\sigma = 5$ Å on the centroid rather than each bead has a negligible effect on the computed properties of the room-temperature liquid, yet it reduces the computational effort to close to that of a classical simulation in the limit of large system size (59). Ring-polymer

contraction therefore makes large-scale RPMD (and indeed PIMD) simulations of systems described by empirical force fields entirely feasible. A more complete discussion of the ring-polymer contraction scheme just outlined is given in Reference 59, the contraction to a ring polymer with an intermediate number of beads is discussed in Reference 58, and a generalized ring-polymer contraction scheme for systems with polarizable force fields is described in Reference 60.

It would clearly be a great deal more difficult to construct a ring-polymer contraction scheme for an ab initio force field, which does not separate so conveniently into short- and long-range contributions. There has, however, been some exciting recent progress in finding alternative ways to make path integral simulations with ab initio force fields more tractable. This can be done efficiently for small systems by adopting a higher-order (more rapidly convergent) path integral discretization (61, 62) and for arbitrarily large systems by accelerating the convergence of the standard discretization with respect to the number of beads by augmenting its dynamics with a generalized Langevin equation (63, 64). Significant progress has been made in both these directions, although so far only for the calculation of static equilibrium properties using PIMD.

### 3.3. Sampling Rare Events

Because they are based on classical MD in an extended phase space, essentially all the techniques developed over the years for performing classical MD simulations can in principle be adopted and used to improve the efficiency of RPMD and PIMD. These include even the comparatively sophisticated techniques that have now been developed to improve the sampling of rare events, such as milestoning (65), transition path sampling (66), and metadynamics (67).

In fact, there are already several examples in the literature of the use of one of the earliest rare-event techniques to facilitate RPMD calculations. An activated chemical reaction is a rare event at low temperatures, at which there is only a small probability that a spontaneous thermal fluctuation will bring the system to the top of the reaction barrier. In principle, one could calculate the RPMD rate simply by running an ensemble of RPMD trajectories from the equilibrated reactant phase space and waiting to see how long they take (on average) to react—and this would give the correct result. However, it would be a highly inefficient way to proceed at low temperatures. A far more practical way to calculate the rate is to use the theory outlined in Section 2.4 and, in particular, the expression for $k^{\mathrm{RPMD}}(T)$ in Equation 35.

This expression is a product of two factors: a statistical QTST rate coefficient $k^{\mathrm{QTST}}(T)$ and a dynamical transmission coefficient $\kappa = \lim_{t\to\infty}\kappa(t)$. The classical Bennett-Chandler method (68, 69) can easily be adapted to calculate the first of these factors from a thermodynamic integration along a reaction coordinate from the reactant region to the transition state, and the second factor can be calculated by initiating an ensemble of RPMD trajectories on the transition-state dividing surface $s(\mathbf{q}) = 0$ and following them to see whether they react. This is how the vast majority of RPMD rate calculations have been performed to date. Full implementational details are given for condensed-phase reactions in References 22, 23, 34, and 35 and for gas-phase reactions in References 27, 33, and 70.

There is also already at least one instance in the literature in which transition path sampling of the reactive RPMD ensemble has been used to shed light on the mechanism of a chemical reaction (35), and we expect to see many more calculations of this sort in the future.

## 4. APPLICATIONS

In the previous sections, we have outlined the formal properties and efficient implementation of RPMD. We now review illustrative applications of the method to a range of molecular systems and dynamical processes.

### 4.1. Dynamics in Liquid Hydrogen

The earliest condensed-phase simulations using RPMD explored the self-diffusion of low-temperature liquid *para*-hydrogen (19), a benchmark system that has been investigated using numerous approximate quantum dynamical methods (71–75). RPMD simulations revealed that the self-diffusion coefficient depends significantly on the size of the simulation cell, showing that it can be misleading to compare the results of different quantum dynamical methods obtained using different system sizes. The system-size effect, which was originally identified in classical simulations of dilute polymers (76) and neat liquids (77), arises from the hydrodynamic interaction of each particle with its periodic images. The discovery of the effect in a quantum simulation was made possible by (*a*) the efficiency of RPMD, which enabled the rapid simulation of multiple system sizes with small statistical uncertainty, and (*b*) the preservation of the quantum Boltzmann distribution in RPMD, which allowed long, microcanonical trajectories to capture the multiple timescale effects associated with the coupling between individual particle diffusion and collective motions in the liquid.

This study of *para*-hydrogen also illustrated the importance of including quantum statistical effects in the simulation of liquid dynamics (19, 78). For *NVT* simulations performed at thermodynamic state points associated with low external pressure, quantum dispersion dictates whether the system lies in the liquid phase or the liquid-vapor coexistence region of the phase diagram (78). Classical trajectories that neglect the effective swelling of the molecules owing to nuclear quantum effects were shown to phase separate, developing a sizable bubble in the simulation cell and exhibiting substantial artifacts in the calculated self-diffusion coefficient; the automatic inclusion of quantum dispersion in RPMD simulations avoids such problems (19).

### 4.2. Dynamics in Liquid Water

Liquid water, even at ambient temperatures, presents a more challenging condensed-phase problem for quantum simulation methods, as it exhibits a broad spectrum of coupled timescales that ranges from high-frequency O-H stretches to low-frequency librations and diffusive modes.

The first application of RPMD to liquid water employed the rigid simple point-charge SPC/E model of water under ambient conditions (20). Previous work had thoroughly characterized changes in the static properties of water due to tunneling and ZPE (79, 80), yet only a handful of studies had probed such effects on the dynamics of water (81–84). In broad agreement with other simulation methods, the rigid-water RPMD simulations predicted an approximately 30% decrease in the timescales for orientational relaxation and translational diffusion due to quantum effects. The faster dynamics observed upon quantization of these water models arises from the fact that ZPE and tunneling in the (low-inertia) orientational degrees of freedom lead to more rapid reorganization of the hydrogen-bonding network and increased translational diffusion (20). As in the study of liquid *para*-hydrogen, the RPMD water simulations also revealed a pronounced system-size dependence of the self-diffusion coefficient due to hydrodynamic effects (20).

A more recent RPMD study has revealed that simulations based on rigid models capture only half the story of quantum effects in liquid water (28). Using the flexible q-TIP4P/F water model, Habershon et al. found that quantization of the anharmonic O-H stretching modes actually counteracts the enhanced diffusivity arising from quantized orientational motion. Quantum ZPE increases the length of the anharmonic O-H bond, which correspondingly increases the molecular dipole moment and causes a tightening of the hydrogen-bonding network in the liquid (85); this tightening partially mitigates the enhancement in water diffusivity upon quantization. The combined impact of quantum effects on the self-diffusion coefficient of the flexible water model

is only a 15% increase, approximately half of that observed for the rigid water model. Recent studies have shown that these competing quantum effects also arise in other hydrogen-bonded systems (86) and that they are fundamentally connected to the experimentally observed isotopic fractionation of hydrogen between the liquid and vapor phases of water (87).

Quantum simulations of flexible liquid water also provide insight from a methodological perspective. In comparison to the modest increase in water diffusivity upon quantization predicted from RPMD (28), simulations performed using the LSC-IVR predict an effect that is approximately three times larger (88). This discrepancy has since been traced to an artifact of the LSC/IVR methodology: Unphysical ZPE leakage from the initially quantized vibrational modes in the semiclassical dynamics leads to heating of the low-frequency diffusive modes at a rate of 470 K $ps^{-1}$ over the first 0.5 ps (29). RPMD simulations avoid such problems by being consistent with the exact quantum mechanical equilibrium distribution.

### 4.3. Zero-Point Energy Effects

Normal and inverse kinetic isotope effects provide a useful way to characterize reactive processes in molecular systems. Generally speaking, normal isotope effects occur when the transition state is less confined than the reactant species, which results in a decrease in ZPE at the transition state and faster reaction rates upon inclusion of quantum effects, or upon substitution of heavy isotopes with lighter ones. Inverse isotope effects occur when the transition state is more confined than the reactants, which results in an increase in ZPE at the transition state and a reversal of the normal isotopic trend—although when the temperature becomes low enough for tunneling to dominate, the lighter isotopes begin to react faster than the heavy ones again.

The ability of RPMD to accurately describe inverse isotope effects was first demonstrated for diffusion-controlled reactions of hydrogen isotopes in water (23). At 300 K, classical MD simulations predict that muonium, an isotope of hydrogen with approximately one-ninth the mass, diffuses more rapidly through water than either hydrogen or deuterium, owing to its greater Maxwellian root-mean-square velocity; this prediction starkly contradicts experimental results that show all three species to have similar diffusion constants. Inclusion of nuclear quantization via the RPMD method, however, leads to relative diffusion rates that are in much better agreement with experiment. The quantum effect here is clearly an inverse kinetic isotope effect, as switching on quantum fluctuations inhibits the diffusion of muonium more than that of hydrogen. In the ring-polymer picture, inverse isotope effects occur because the ring polymers of lighter atoms are more swollen than those of heavy atoms at the same temperature, and their motion through confined regions of space is therefore more strongly inhibited (23).

At 8 K, where the diffusion of interstitial atoms in ice is governed by tunneling-mediated hopping between neighboring cavities in the ice structure, RPMD was found to yield a muonium intercavity hopping rate within a factor of three of the experimental value (23). Because of the extreme quantum nature of this process, the RPMD hopping rate for hydrogen was found to be ten orders of magnitude smaller than that for muonium, and indeed the diffusion of hydrogen atoms in ice has not been observed experimentally below 40 K (23).

An even richer diversity of dynamical behavior was observed in an application of RPMD to a binary supercooled liquid near its glass transition (36, 39). **Figure 1** presents the calculated diffusion coefficient of a tagged particle in the liquid as a function of $\Lambda^*$, the ratio of the thermal de Broglie wavelength of the particle to its diameter. As quantum mechanical effects are switched on by increasing $\Lambda^*$ from 0, the diffusion coefficient is initially unchanged because a modest swelling of the ring polymers is accommodated by the available space between the particles (**Figure 1*a***). However, a further increase in $\Lambda^*$ leads to a marked decrease in the diffusion constant because

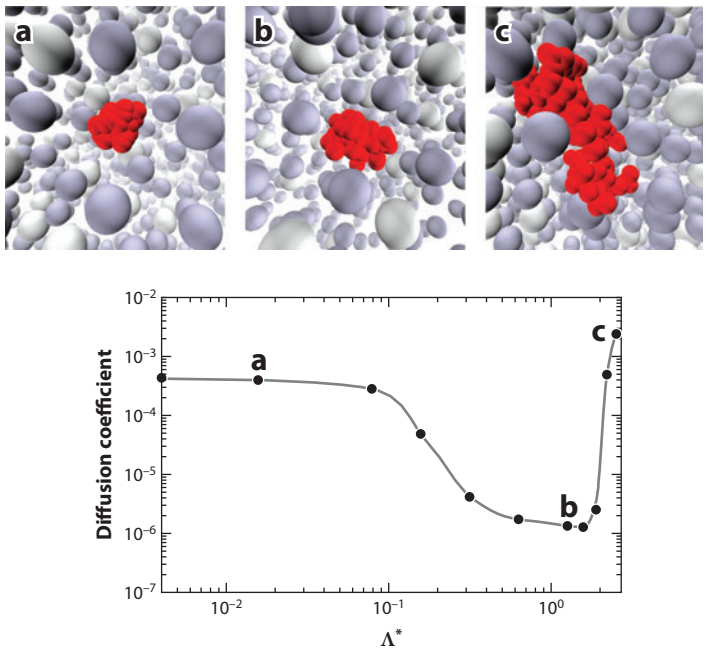


**Figure 1**

The ring-polymer molecular dynamics (RPMD) self-diffusion coefficient of a particle in a glassy binary fluid as a function of the magnitude of quantum fluctuations in the system, characterized by $\Lambda^*$, the ratio of the thermal de Broglie wavelength of the particle to its diameter (36, 39). All quantities are reported in reduced units. Panels *a–c* show snapshots taken from the simulations at three different values of $\Lambda^*$. For clarity, the full ring polymer is only shown for one particle (*red*), and all other particles are represented by their centroids. Figure adapted from References 36 and 39.

the ring polymers are more swollen and must now push past each other to diffuse (**Figure 1*b***). Finally, in the regime of large $\Lambda^*$, the diffusion constant again increases as the diffusion becomes dominated by quantum tunneling, and the quantized particles delocalize across multiple solvation sites in the liquid (**Figure 1*c***).

Yet another example is provided by the $Mu + H_2 \rightarrow MuH + H$ gas-phase reaction, which exhibits a notoriously large inverse kinetic isotope effect because of the difference in ZPE between its reactants and products. Throughout the temperature range 200–1,000 K, the RPMD rate coefficient for this reaction is found to be within 5% of the exact quantum mechanical result (37). This is a case in which the RPMD rate is uncharacteristically accurate, reflecting just how well the method captures ZPE effects. More typical RPMD results for gas- and condensed-phase reactions are discussed in the following section.

## 4.4. Tunneling in Chemical Dynamics

An important application domain for RPMD is the calculation of chemical reaction rates and the analysis of reaction mechanisms in tunneling processes. Initial applications of RPMD to the thermal rate problem addressed standard benchmark systems, including the Eckart barrier (9, 10) and the linearly coupled system-bath model (9). These studies demonstrated various advantageous features of the method, including the insensitivity of the calculated reaction rate to the choice dividing surface, the accurate description of both shallow- and deep-tunneling regimes, and the

correct prediction of the Kramers' turnover effect upon increased coupling between the reactive system and its environment (9).

Rate calculations in gas-phase molecular systems provide a practical realization of the formal connections between RPMD and semiclassical instanton theory (40). For the symmetric $H + H_2$ reaction, classical MD predicts a reaction rate at 200 K that is more than three orders of magnitude smaller than the exact result (27); RPMD simulations yield a rate that is only 21% lower than the exact result, in accordance with the expectation that the method slightly underestimates rates for deep tunneling across a symmetric barrier (40). For the asymmetric $H + CH_4$ reaction, RPMD somewhat overestimates the low-temperature reaction rate, which is also anticipated from its connection to instanton theory (33, 40). However, even at 225 K, for which classical MD is in error by three orders of magnitude, RPMD remains within a factor of two of the exact result.

In addition to providing good accuracy in comparison with known exact results, RPMD substantially expands the range of feasible calculation of quantized reaction rates. For example, it is not currently possible to converge the exact quantum rate calculation for the $H + CH_4$ system above 400 K, a regime of primary interest in hydrocarbon combustion chemistry. However, RPMD rate calculations capture the essential quantum mechanical features of this reaction and were readily converged at temperatures ranging from 200 K to 2,000 K (33).

Reactive tunneling in condensed-phase molecular systems has also been studied using RPMD. The earliest such application addressed the proton transfer reaction between phenol and trimethylamine in a polar solvent at 249 K (22). Quantum tunneling and ZPE effects play an important role in this reaction, augmenting the classical rate by approximately four orders of magnitude. Interestingly, the calculated RPMD proton transfer rate for this system is several times smaller than those of various other quantum dynamics methods that have been applied to the problem (89–93). As there are no exact results for this system, assessment of the relative accuracy for the various methods is not possible. However, unlike the other methods applied to this system, RPMD rigorously accounts for trajectory recrossing associated with a given choice of dividing surface. The degree of trajectory recrossing was used to assess the relative quality of different transition-state descriptions for the reaction, and it was shown that solvent polarization provides a better reaction coordinate than one based on the donor-proton-acceptor bond lengths in the system.

Finally, in the largest-scale application of RPMD to date, the method was employed to investigate hydride transfer in *Escherichia coli* dihydrofolate reductase (DHFR) (35), an important prototype for the role of protein motions in enzyme catalysis (see **Figure 2**). By combining RPMD with transition path sampling methods (66), Boekelheide et al. generated the full ensemble of reactive trajectories and distinguished between the effects of statistical and dynamical correlations on the hydride transfer mechanism. This analysis conclusively demonstrated that although protein motions are statistically correlated with the hydride transfer over a length scale of nanometers, dynamical correlations decay on much shorter length scales, essentially vanishing at distances of 4–6 Å from the transferring hydride. In addition, RPMD simulations confirm that quantum tunneling enhances the hydride transfer rate in DHFR by approximately three orders of magnitude. The success of this study emphasizes that RPMD is a promising tool for advancing the mechanistic understanding of enzymatic reactions involving hydrogen transfer, electron transfer, or proton-coupled electron transfer processes, for which kinetic isotope effects play a key role in connecting theory with experiment (94–96).

## 5. LIMITATIONS

Despite the success of the applications described above, RPMD does have some important limitations. These include the presence of unphysical frequencies in calculated spectra, a related issue

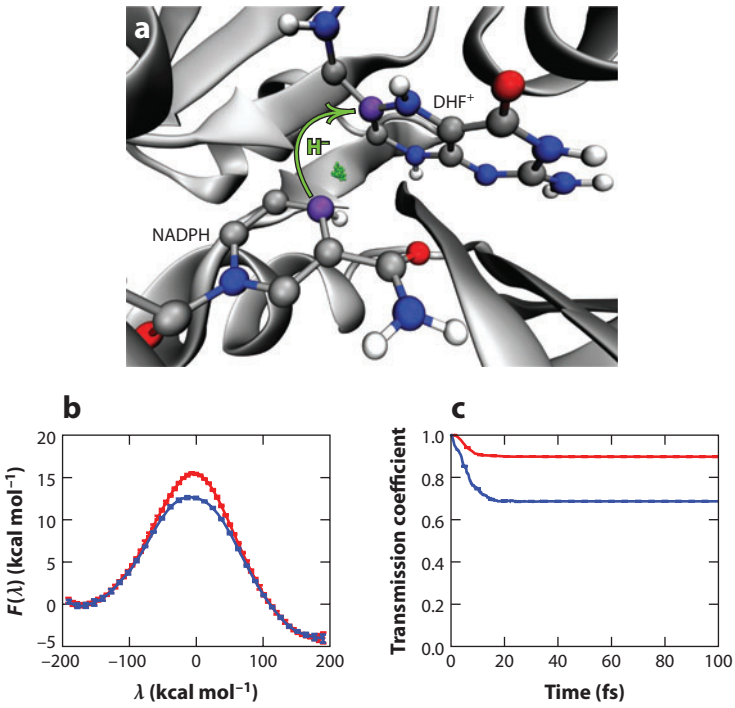


**Figure 2**

The hydride transfer reaction catalyzed by DHFR. (*a*) The enzyme active site is shown with the hydride (*green*) in the ring-polymer representation and with the donor and acceptor carbon atoms in purple. (*b*) The free-energy profile for the reaction, obtained using classical molecular dynamics (MD) (*red*) and ring-polymer molecular dynamics (RPMD) (*blue*). (*c*) The time-dependent transmission coefficient corresponding to the dividing surface at the free-energy maximum, obtained using classical MD (*red*) and RPMD (*blue*). Figure adapted from Reference 35.

that arises when calculating the correlation functions of nonlinear operators, and problems arising from the neglect of real-time quantum coherence in the dynamics. In this section, we discuss each issue in turn and use them to highlight the situations in which RPMD is unreliable.

## 5.1. Spurious Frequencies

After a normal mode transformation (57, 58, 97), the ring-polymer Hamiltonian for a one-dimensional harmonic oscillator with frequency $\omega$ can be written as

$$H_n(\tilde{\mathbf{p}}, \tilde{\mathbf{q}}) = \sum_{k=0}^{n-1} \left[ \frac{\tilde{p}_k^2}{2m} + \frac{1}{2} m \omega_k^2 \tilde{q}_k^2 \right], \tag{54}$$

where

$$\omega_k = \sqrt{\omega^2 + (2n/\beta\hbar)^2 \sin^2(k\pi/n)}. \tag{55}$$

In RPMD, the centroid mode ($k = 0$) therefore oscillates at the harmonic frequency $\omega$, whereas the other normal modes oscillate at higher frequencies that depend on the number of beads and on the temperature. These internal-mode oscillations are unrelated to the dynamics of the physical potential; they are artificial oscillations that arise from the structure of the extended phase space.

In many applications, the high-frequency oscillations of the ring polymer do not matter because they are well separated from the dynamics of physical interest. For example, diffusion coefficients are the zero-frequency components of velocity autocorrelation spectra, and chemical reaction rates are the zero-frequency components of reactive flux autocorrelation spectra. However, problems do arise when using RPMD to calculate absorption spectra in systems containing high-frequency physical vibrations (26), as illustrated by a recent RPMD simulation of the dipole absorption spectrum of room-temperature liquid water (97).

In this simulation, the RPMD approximation was found to give good agreement with the experimental absorption spectrum in the low-frequency librational and intermediate-frequency water bending regions but poor agreement in the high-frequency O-H stretching region (97). An analysis of the calculation showed that the stretching region of the spectrum was contaminated by the internal modes of the ring polymer, resulting in a series of spurious peaks with strongly temperature-dependent frequencies (97). It was also shown how the contamination could be removed by decreasing the masses of the internal modes so as to push the spurious frequencies beyond the spectral range of interest, as done in the partially adiabatic implementation of CMD (74).

The lesson to be learned from this is that the spectral information produced by RPMD is not to be trusted at frequencies above the first free ring-polymer excitation frequency, $\omega_1 = (2n/\beta\hbar)\sin(\pi/n) \simeq 2\pi/\beta\hbar$, which corresponds to a wave number of approximately 1,300 $\text{cm}^{-1}$ at 300 K (98). Among other things, this precludes the use of RPMD to calculate the high-frequency components of the force-force autocorrelation spectra that govern the relaxation rates of vibrationally excited molecules in liquids (99, 100), and the adiabatic CMD modification does not seem to help in this case (101).

## 5.2. The Nonlinear Operator Problem

A second important limitation of RPMD is its poor performance for the correlation functions of nonlinear operators. Let us consider the calculation of correlation functions for the simple harmonic oscillator, $V(q) = \frac{1}{2}m\omega^2 q^2$. RPMD gives the exact quantum mechanical result when one of the correlated operators is a linear function of position or momentum (8). However, in the case of the nonlinear operator $\hat{q}^2$, the exact quantum mechanical Kubo-transformed autocorrelation function is (102)

$$\tilde{c}_{q^2q^2}(t) = \left(\frac{\hbar}{2m\omega}\right)^2 \left[\frac{2}{\beta\hbar\omega}\coth\frac{\beta\hbar\omega}{2}\cos 2\omega t + 2\coth^2\frac{\beta\hbar\omega}{2} - 1\right], \tag{56}$$

whereas the RPMD result is (102)

$$\tilde{c}_{q^2q^2}(t) \simeq \frac{1}{(\beta m)^2}\left[\sum_{k=0}^{n-1}\frac{1}{\omega_k^4}(\cos 2\omega_k t + 1) + \sum_{k=0}^{n-1}\sum_{l=0}^{n-1}\frac{1}{\omega_k^2\omega_l^2}\right], \tag{57}$$

where $\omega_k$ and $\omega_l$ are defined in Equation 55. From these equations, we see that, although the RPMD autocorrelation function does have a component ($k = 0$) that oscillates at the correct frequency ($2\omega$), there are additional, spurious components that arise from the internal modes of the ring polymer and contaminate the time signal (102).

This difficulty with nonlinear operators is not restricted to simple model problems: It can also appear in real-world applications. An interesting example is provided by RPMD simulations of the inelastic neutron scattering from liquid *para*-hydrogen (21). Here incoherent dynamic structure factors were calculated by correlating the nonlinear operators $e^{\pm i\boldsymbol{\kappa}\cdot\hat{\boldsymbol{q}}_i}$. For low values of the momentum transfer $\hbar|\boldsymbol{\kappa}|$, these operators are approximately linear functions of the position operator $\hat{\boldsymbol{q}}_i$, and RPMD gives good agreement with experimental data. However, as $|\boldsymbol{\kappa}|$ increases,

the correlated operators become increasingly nonlinear, and the calculated dynamic structure factors become contaminated by the ring-polymer internal modes.

The problem can be avoided in the case of incoherent neutron scattering by adopting the well-known Gaussian approximation to the self part of the intermediate scattering function (103), which depends only on the velocity autocorrelation function and is therefore accurately calculated by RPMD (21). More generally, the nonlinear operator problem can be mitigated to a large extent in low-temperature systems such as liquid *para*-hydrogen by using maximum entropy analytic continuation (MEAC) techniques (104–109) to refine the RPMD correlation function (75). Because analytic continuation is most effective at low temperatures where the thermal time $\beta\hbar$ is long (110), and the RPMD prior becomes exact at high temperatures where the analytic continuation is ineffective, the RPMD and MEAC methods are complementary, and the combination of the two is better than either in isolation (75). Moreover, the imaginary-time data that are used as input for the analytic continuation can be extracted directly from the RPMD trajectories.



### 5.3. Lack of Real-Time Coherence

The central assumption of the RPMD approach is that real-time quantum coherences dissipate rapidly in condensed-phase chemical systems. By sampling the exact quantum Boltzmann distribution, the method rigorously includes quantum statistical effects such as ZPE and static tunneling, but the lack of phase information in the RPMD equations of motion clearly prohibits the description of quantum coherences that persist beyond the thermal time $\beta\hbar$.

As evidenced by the successful applications of the RPMD method described in Section 4, this assumption generally holds for condensed-phase chemical systems at ambient temperatures. However, notable breakdowns have been identified and characterized for gas-phase scattering processes (25) and for electron transfer (ET) in the Marcus inverted regime (34).

The effect of dissipative solvent interactions on the accuracy of the method is illustrated by a study of the diffusive dynamics of an excess electron in supercritical fluid helium at various densities (25). Using a one-electron pseudopotential to describe the electron-helium interactions, the dynamics of the excess electron was considered over a broad range of fluid densities, and the accuracy of the RPMD model was tested against numerically exact path integral statistics through the use of MEAC techniques. At densities typical of dense liquids, the RPMD correlation functions were found to be in excellent agreement with the analytical continuation constraints. In this regime, the electron is strongly localized in a solvent cavity and exhibits a large energy gap between its ground- and first-excited electronic states; the dominant quantum effects in this regime are ZPE and tunneling effects associated with electron hopping between neighboring solvent cavities. At lower densities, however, the excess electron exhibits coherent quantum dynamics as it cascades off of dilute helium scatterers; in this regime, the RPMD dynamics deviates substantially from the results that include the MEAC correction. This deviation accompanies the breakdown of the underlying assumptions of RPMD.

The strengths and weaknesses of the method are also illustrated by its performance for ET reactions. The accuracy of RPMD was recently investigated in the context of mixed-valence ET reactions in water, where it was compared with the predictions of Marcus theory (111), semiclassical instanton theory, and exact quantum dynamics calculations (34). Simulations were performed using all-atom potential energy surfaces that include explicit water molecules and electron-molecule pseudopotentials (112), as well as with system-bath models for ET in a polar solvent.

**Figure 3** compares thermal rate constants obtained using RPMD and Marcus theory for mixed-valence ET reactions as a function of the thermodynamic driving force (34). This comparison includes no adjustable parameters, emphasizing that the RPMD reaction rates are in excellent

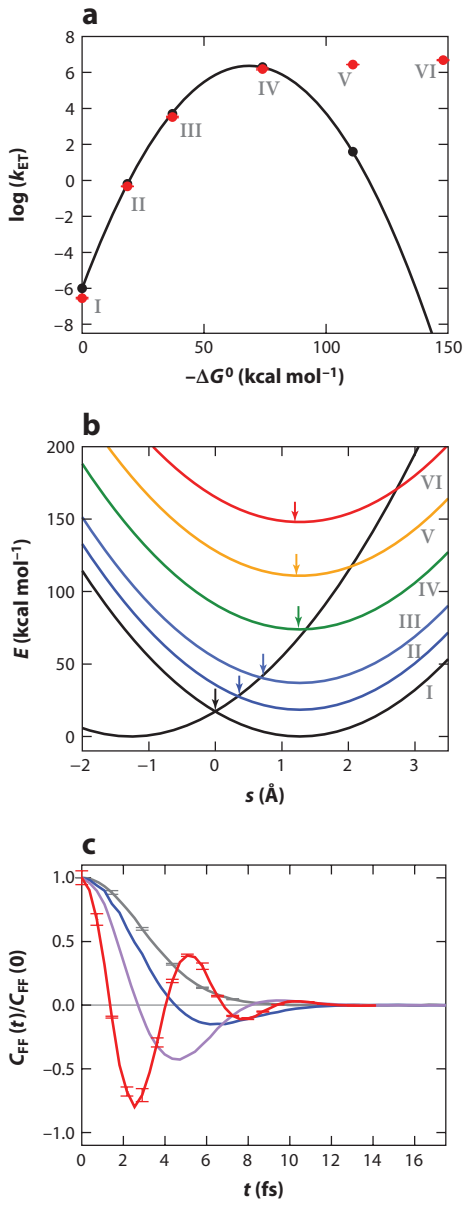


**Figure 3**

(*a*) Ring-polymer molecular dynamics (RPMD) (*red*) and Marcus theory (*black*) rates for mixed-valence electron transfer (ET) in liquid water as a function of the thermodynamic driving force for the reaction. Excellent agreement is found throughout the normal and barrierless regimes for electron transfer. Deviations in the inverted regime result from the important role of electronic-state resonance in the real-time dynamics. (*b*) Marcus parabolas for the reactant (*right*) and product (*left*) electronic diabats as a function of the solvent polarization, *s*. The arrows indicate the solvent configurations that maximally contribute to the RPMD ET rate. (*c*) Normalized flux-flux autocorrelation functions for ET at various thermodynamic driving forces, calculated using exact quantum dynamics for cases I (*black*), II (*blue*), III (*purple*), and IV (*red*). Figure adapted from Reference 34.

agreement with the predictions of Marcus theory throughout the normal and activationless regimes for ET ($-\Delta G^\circ < 70$ kcal mol$^{-1}$ in this system). However, the figure also demonstrates that the success of the RPMD method does not extend into the Marcus inverted regime. The RPMD rates are seen to be only weakly dependent on the increasing driving force in the inverted regime ($-\Delta G^\circ >$ 70 kcal mol$^{-1}$), rather than exhibiting the characteristic turnover predicted by Marcus theory.

Deviation of the RPMD results from Marcus theory in the inverted regime is also clear upon inspection of the calculated ET mechanism (34). **Figure 3*b*** presents the free-energy parabolas for the reactant and product electronic diabats as a function of the solvent polarization; also indicated are the solvent configurations that maximally contribute to the ET rate. In the normal and activationless regimes, RPMD correctly predicts an ET transition state at the crossing of the electronic diabats. However, in the inverted regime, the ET transition-state configurations are predominantly located at the minimum of the reactant basin. RPMD (as well as the closely related semiclassical instanton theory) significantly overestimates the tunneling probability between asymmetric basins, leading to an incorrect ET mechanism and an overestimation of the reaction rate in the inverted regime.

**Figure 3*c*** shows that resonance features in the real-time dynamics are critical for capturing the dynamics of the inverted regime (34). The figure presents flux-flux correlation functions obtained using numerically exact quantum dynamics methods. At larger thermodynamic driving forces, the correlation functions become increasingly oscillatory, with a resonance frequency that matches the electronic state energy gap between the ET reactant and product (113, 114). Integration over this increasingly oscillatory time-correlation function contributes to the turnover in the ET reaction rate in the inverted regime. The RPMD approximation to the real-time dynamics of the system, which is not expected to capture coherent quantum effects (8, 25), does not fully enforce the quantization of electronic dynamics and leads to the observed inaccuracies in the inverted regime. Approximate quantum dynamical methods that explicitly enforce electronic quantization either by using a discrete electronic state basis or by exactly mapping to a continuous electronic basis are thus expected to provide a better starting point for describing state-to-state electronic dynamics and ET in the inverted regime (115–119). However, such methods typically suffer from the drawback of not preserving the quantum Boltzmann distribution (120, 121).

These applications to electron diffusion and ET dynamics present clear cases in which the RPMD method fails to capture the essential physics of the problem. However, both applications are also encouraging from a practical perspective, given that excellent results are obtained throughout the regimes of primary chemical relevance. For the electron diffusion simulations, RPMD is fully consistent with the dynamics predicted via analytical continuation in the solvent density regime that corresponds to condensed-phase systems. In the ET simulations, RPMD predicts both the reaction mechanisms and thermal rate constants across 13 orders of magnitude in the normal and activationless regimes, which encompass the vast majority of ET reactions in biological and synthetic systems (122). Thus, although these applications clearly illustrate the limitations of RPMD, they also emphasize that the method is a powerful tool for the direct simulation of reactive processes in chemically relevant regimes.

## 6. OUTLOOK

In many regards, RPMD is now a mature and accessible technology that enables the quantization of MD trajectories in complex systems containing many interacting particles. It has been implemented in several widely used MD simulation packages (123, 124), and it has been benchmarked and its potential demonstrated in numerous applications spanning a wide range of regimes. Needless to say, as with any approximate method, RPMD does have its limitations, and there is

room to improve its accuracy and breadth of applicability. But for a large class of problems, the method is already useful, and it is our hope that this review provides a solid foundation for an expanded community to employ RPMD in future chemical and physical applications.

A central focus of future work will be to improve the interface between electronic and nuclear dynamics in the RPMD framework. The efficient combination of RPMD with ab initio electronic structure methods offers a powerful way forward for the quantitative, first-principles description of many molecular processes. A generalization of RPMD that goes beyond the standard position representation of the imaginary-time path integral might open the door to a more general and accurate description of state-to-state electronic transitions and nonadiabatic reaction dynamics. Finally, a systematic derivation of the RPMD approach would provide a valuable foundation for new methodological developments. These and other challenges present an exciting and full landscape for future research.

## DISCLOSURE STATEMENT

The authors are not aware of any affiliations, memberships, funding, or financial holdings that might be perceived as affecting the objectivity of this review.

## ACKNOWLEDGMENTS

S.H. acknowledges the Leverhulme Trust for the award of an Early Career Fellowship and the EPSRC for funding under program grant EP/G00224X. D.E.M. acknowledges support from the Miller Institute at the University of California, Berkeley, and from the Wolfson Foundation and the Royal Society. T.E.M. acknowledges support from Stanford University. T.F.M. acknowledges the US Office of Naval Research (USONR) under grant N00014-10-1-0884, National Science Foundation (NSF) CAREER Award under grant CHE-1057112, the US Army Research Laboratory and the US Army Research Office under grant W911NF-10-1-0202, and the US Department of Energy (DOE), Chemical Sciences, Geosciences and Biosciences Division, Office of Basic Energy Sciences under grant DE-FG02-11ER16247. We are extremely grateful to David Chandler for his insights and support throughout the development of RPMD, and we are indebted to the many people who have made valuable contributions to the work described in this review: Ian Craig, Bas Braams, Rosana Collepardo-Guevara, George Fanourgakis, Yury Suleimanov, Michele Ceriotti, Nandini Ananth, Artur Menzeleev, Nicholas Boekelheide, Joshua Kretchmer, and Romelia Salomón-Ferrer.

## LITERATURE CITED

1. Allen MP, Tildesley DJ. 1987. *Computer Simulation of Liquids*. New York: Oxford Univ. Press
2. Frenkel D, Smit B. 2002. *Understanding Molecular Simulation: From Algorithms to Applications*. San Diego: Academic
3. Wang H, Sun X, Miller WH. 1998. Semiclassical approximations for the calculation of thermal rate constants for chemical reactions in complex molecular systems. *J. Chem. Phys.* 108:9726–36
4. Sun X, Wang H, Miller WH. 1998. Semiclassical theory of electronically nonadiabatic dynamics: results of a linearized approximation to the initial value representation. *J. Chem. Phys.* 109:7064–74
5. Liu J, Miller WH. 2007. Linearized semiclassical initial value time correlation functions using the thermal Gaussian approximation: applications to condensed phase systems. *J. Chem. Phys.* 127:114506
6. Cao J, Voth GA. 1994. The formulation of quantum statistical mechanics based on the Feynman path centroid density. II. Dynamical properties. *J. Chem. Phys.* 100:5106–17

7. Jang S, Voth GA. 1999. A derivation of centroid molecular dynamics and other approximate time evolution methods for path integral centroid variables. *J. Chem. Phys.* 111:2371–84
8. Craig IR, Manolopoulos DE. 2004. Quantum statistics and classical mechanics: real time correlation functions from ring polymer molecular dynamics. *J. Chem. Phys.* 121:3368–73
9. Craig IR, Manolopoulos DE. 2005. Chemical reaction rates from ring polymer molecular dynamics. *J. Chem. Phys.* 122:084106
10. Craig IR, Manolopoulos DE. 2005. A refined ring polymer molecular dynamics theory of chemical reaction rates. *J. Chem. Phys.* 123:034102
11. Braams BJ, Manolopoulos DE. 2006. On the short-time limit of ring polymer molecular dynamics. *J. Chem. Phys.* 125:124105
12. Chandler D, Wolynes PG. 1981. Exploiting the isomorphism between quantum theory and classical statistical mechanics of polyatomic fluids. *J. Chem. Phys.* 74:4078–95
13. Wang HB, Thoss M, Sorge KL, Gelabert R, Giminez X, Miller WH. 2001. Semiclassical description of quantum coherence effects and their quenching: a forward-backward initial value representation study. *J. Chem. Phys.* 114:2562–71
14. Gelabert R, Giminez X, Thoss M, Wang HB, Miller WH. 2001. Semiclassical description of diffraction and its quenching by the forward-backward version of the initial value representation. *J. Chem. Phys.* 114:2572–79
15. Miller WH. 2012. Perspective: quantum or classical coherence? *J. Chem. Phys.* 136:210901
16. Voth GA. 1996. Path-integral centroid methods in quantum statistical mechanics and dynamics. *Adv. Chem. Phys.* 93:135–218
17. Miller WH. 2001. The semiclassical initial value representation: a potentially practical way for adding quantum effects to classical molecular dynamics simulations. *J. Phys. Chem. A* 105:2942–55
18. Thoss M, Wang H. 2004. Semiclassical description of molecular dynamics based on initial-value representation methods. *Annu. Rev. Phys. Chem.* 55:299–332
19. Miller TF, Manolopoulos DE. 2005. Quantum diffusion in liquid *para*-hydrogen from ring polymer molecular dynamics. *J. Chem. Phys.* 122:184503
20. Miller TF, Manolopoulos DE. 2005. Quantum diffusion in liquid water from ring polymer molecular dynamics. *J. Chem. Phys.* 123:154504
21. Craig IR, Manolopoulos DE. 2006. Inelastic neutron scattering from liquid *para*-hydrogen by ring polymer molecular dynamics. *Chem. Phys.* 322:236–46
22. Collepardo-Guevara R, Craig IR, Manolopoulos DE. 2008. Proton transfer in a polar solvent from ring polymer reaction rate theory. *J. Chem. Phys.* 128:144502
23. Markland TE, Habershon S, Manolopoulos DE. 2008. Quantum diffusion of hydrogen and muonium atoms in liquid water and hexagonal ice. *J. Chem. Phys.* 128:194506
24. Hone TD, Poulsen JA, Rossky PJ, Manolopoulos DE. 2008. Comparison of approximate quantum simulation methods applied to normal liquid helium at 4 K. *J. Phys. Chem. B* 112:294–300
25. Miller TF. 2008. Isomorphic classical molecular dynamics model for an excess electron in a supercritical fluid. *J. Chem. Phys.* 129:194502
26. Shiga M, Nakayama A. 2008. Ab initio path integral ring polymer molecular dynamics: vibrational spectra of molecules. *Chem. Phys. Lett.* 451:175–81
27. Collepardo-Guevara R, Suleimanov YV, Manolopoulos DE. 2009. Bimolecular reaction rates from ring polymer molecular dynamics. *J. Chem. Phys.* 130:174713
28. Habershon S, Markland TE, Manolopoulos DE. 2009. Competing quantum effects in the dynamics of a flexible water model. *J. Chem. Phys.* 131:024501
29. Habershon S, Manolopoulos DE. 2009. Zero point energy leakage in condensed phase dynamics: an assessment of quantum simulation methods for liquid water. *J. Chem. Phys.* 131:244518
30. Shiga M, Kaczmarek A, Marx D. 2009. Quantum effects on vibrational and electronic spectra of hydrazine studied by on-the-fly ab initio ring polymer molecular dynamics. *J. Phys. Chem. A* 113:1985–94
31. Menzeleev AR, Miller TF. 2010. Ring polymer molecular dynamics beyond the linear response regime: excess electron injection and trapping in liquids. *J. Chem. Phys.* 132:034106
32. Calvo F, Costa D. 2010. Diffusion of hydrides in palladium nanoclusters: a ring polymer molecular dynamics study of quantum finite size effects. *J. Chem. Theory Comput.* 6:508–16

33. Suleimanov YV, Collepardo-Guevara R, Manolopoulos DE. 2011. Bimolecular reaction rates from ring polymer molecular dynamics: application to $H + CH_4 \rightarrow H_2 + CH_3$. *J. Chem. Phys.* 134:044131
34. Menzeleev AR, Ananth N, Miller TF. 2011. Direct simulation of electron transfer using ring polymer molecular dynamics: comparison with semiclassical instanton theory and exact quantum methods. *J. Chem. Phys.* 135:074106
35. Boekelheide N, Salomon-Ferrer R, Miller TF. 2011. Dynamics and dissipation in enzyme catalysis. *Proc. Natl. Acad. Sci. USA* 108:16159–63
36. Markland TE, Morrone JA, Berne BJ, Miyazaki K, Rabani E, Reichman DR. 2011. Quantum fluctuations can promote or inhibit glass formation. *Nat. Phys.* 7:134–37
37. Perez de Tudela R, Aoiz FJ, Suleimanov YV, Manolopoulos DE. 2012. Chemical reaction rates from ring polymer molecular dynamics: zero point energy conservation in $Mu + H_2 \rightarrow MuH + H$. *J. Phys. Chem. Lett.* 3:493–97
38. Suleimanov YV. 2012. Surface diffusion of hydrogen on Ni(100) from ring polymer molecular dynamics. *J. Phys. Chem. C* 116:11141–53
39. Markland TE, Morrone JA, Berne BJ, Miyazaki K, Reichman DR, Rabani E. 2012. Theory and simulations of quantum glass forming liquids. *J. Chem. Phys.* 136:074511
40. Richardson JO, Althorpe SC. 2009. Ring polymer molecular dynamics rate theory in the deep tunneling regime: connection with semiclassical instanton theory. *J. Chem. Phys.* 131:214106
41. Zwanzig R. 1965. Time-correlation functions and transport coefficients in statistical mechanics. *Annu. Rev. Phys. Chem.* 16:67–102
42. McQuarrie DA. 2000. *Statistical Mechanics*. Sausalito, CA: Univ. Sci.
43. Miller WH, Schwartz SD, Tromp JW. 1983. Quantum mechanical rate constants for bimolecular reactions. *J. Chem. Phys.* 79:4889–98
44. Kubo R. 1957. Statistical-mechanical theory of irreversible processes. I. General theory and simple applications to magnetic and conduction problems. *J. Phys. Soc. Jpn.* 12:570–86
45. Feynman RP, Hibbs AR. 1965. *Quantum Mechanics and Path Integrals*. New York: McGraw-Hill
46. Parrinello M, Rahman A. 1984. Study of an F center in molten KCl. *J. Chem. Phys.* 80:860–67
47. Chandler D. Theory of quantum processes in liquids. In *Liquids, Freezing and Glass Transition*, Part I, ed. D Levesque, JP Hansen, J Zinn-Justin, pp. 193–285. Les Houches 51. Amsterdam: North Holland
48. Chandler D, Leung K. Excess electrons in liquids: geometrical perspectives. *Annu. Rev. Phys. Chem.* 45:557–91
49. Gillan MJ. 1987. Quantum simulation of hydrogen in metals. *Phys. Rev. Lett.* 58:563–66
50. Gillan MJ. 1987. Quantum-classical crossover of the transition rate in the damped double well. *J. Phys. C* 20:3621–41
51. Voth GA, Chandler D, Miller WH. 1989. Rigorous formulation of quantum transition state theory and its dynamical corrections. *J. Chem. Phys.* 91:7749–60
52. Miller WH. 1975. Semiclassical limit of quantum mechanical transition state theory for nonseparable systems. *J. Chem. Phys.* 62:1899–906
53. Callan CG, Coleman S. 1977. Fate of the false vacuum. II. First quantum corrections. *Phys. Rev. D* 16:1762–68
54. Althorpe SC. 2011. On the equivalence of two commonly used forms of semiclassical instanton theory. *J. Chem. Phys.* 134:114104
55. Hall RW, Berne BJ. 1984. Nonergodicity in path integral molecular dynamics. *J. Chem. Phys.* 81:3641–43
56. Perez A, Tuckerman ME, Muser MH. 2009. A comparative study of the centroid and ring-polymer molecular dynamics methods for approximating quantum time correlation functions from path integrals. *J. Chem. Phys.* 130:184105
57. Ceriotti M, Parrinello M, Markland TE, Manolopoulos DE. 2010. Efficient stochastic thermostatting of path integral molecular dynamics. *J. Chem. Phys.* 133:124104
58. Markland TE, Manolopoulos DE. 2008. An efficient ring polymer contraction scheme for imaginary time path integral simulations. *J. Chem. Phys.* 129:024105
59. Markland TE, Manolopoulos DE. 2008. A refined ring polymer contraction scheme for systems with electrostatic interactions. *Chem. Phys. Lett.* 464:256–61

60. Fanourgakis GS, Markland TE, Manolopoulos DE. 2009. A fast path integral method for polarizable force fields. *J. Chem. Phys.* 131:094102
61. Perez A, Tuckerman ME. 2011. Improving the convergence of closed and open path integral molecular dynamics via higher order Trotter factorization schemes. *J. Chem. Phys.* 135:064104
62. Ceriotti M, Brain GAR, Riordan O, Manolopoulos DE. 2012. The inefficiency of re-weighted sampling and the curse of system size in high-order path integration. *Proc. R. Soc. A* 468:2–17
63. Ceriotti M, Manolopoulos DE, Parrinello M. 2011. Accelerating the convergence of path integral dynamics with a generalized Langevin equation. *J. Chem. Phys.* 134:084104
64. Ceriotti M, Manolopoulos DE. 2012. Efficient first-principles calculation of the quantum kinetic energy and momentum distribution of nuclei. *Phys. Rev. Lett.* 109:100604
65. Faradjian AK, Elber R. 2004. Computing time scales from reaction coordinates by milestoning. *J. Chem. Phys.* 120:10880–89
66. Bolhuis PG, Chandler D, Dellago C, Geissler PL. 2002. Transition path sampling: throwing ropes over rough mountain passes, in the dark. *Annu. Rev. Phys. Chem.* 53:291–318
67. Barducci A, Bonomi M, Parrinello M. 2011. Metadynamics. *Wiley Interdiscip. Rev. Comput. Mol. Sci.* 1:826–43
68. Bennett CH. 1977. Molecular dynamics and transition state theory: the simulation of infrequent events. In *Algorithms for Chemical Computation*, ed. RE Christofferson, pp. 63–97. ACS Symp. Ser. 46. Washington, DC: Am. Chem. Soc.
69. Chandler D. 1978. Statistical mechanics of isomerization dynamics in liquids and the transition state approximation. *J. Chem. Phys.* 68:2959–71
70. Stecher TS, Althorpe SC. 2012. Improved free-energy interpolation scheme for obtaining gas-phase reaction rates from ring polymer molecular dynamics. *Mol. Phys.* 110:875–83
71. Reichman DR, Rabani E. 2002. A self-consistent mode-coupling theory for dynamical correlations in quantum liquids: application to liquid *para*-hydrogen. *J. Chem. Phys.* 116:6279–85
72. Nakayama A, Makri N. 2003. Forward backward semiclassical dynamics for quantum fluids using pair propagators: application to liquid *para*-hydrogen. *J. Chem. Phys.* 119:8592–605
73. Yonetani Y, Kinugawa K. 2003. Transport properties of liquid para-hydrogen: the path integral centroid molecular dynamics approach. *J. Chem. Phys.* 119:9651–60
74. Hone TD, Rossky PJ, Voth GA. 2006. A comparative study of imaginary time path integral based methods for quantum dynamics. *J. Chem. Phys.* 124:154103
75. Habershon S, Braams BJ, Manolopoulos DE. 2007. Quantum mechanical correlation functions, maximum entropy analytic continuation, and ring polymer molecular dynamics. *J. Chem. Phys.* 127:174108
76. Dunweg B, Kremer K. 1993. Molecular dynamics simulation of a polymer chain in solution. *J. Chem. Phys.* 99:6983–97
77. Yeh I-C, Hummer G. 2004. System-size dependence of diffusion coefficients and viscosities from molecular dynamics simulations with periodic boundary conditions. *J. Phys. Chem. B* 108:15873–79
78. Miller TF, Manolopoulos DE, Madden PA, Konieczny M, Oberhofer H. 2005. Comment on a centroid molecular dynamics study of liquid *para*-hydrogen and *ortho*-deuterium. *J. Chem. Phys.* 122:057101
79. Kuharski RA, Rossky PJ. 1984. Quantum mechanical contributions to the structure of liquid water. *Chem. Phys. Lett.* 103:357–62
80. Wallqvist A, Berne BJ. 1985. Path-integral simulation of pure water. *Chem. Phys. Lett.* 117:214–19
81. Lobaugh J, Voth GA. 1997. A quantum model for water: equilibrium and dynamical properties. *J. Chem. Phys.* 106:2400–10
82. Guillot B, Guissani Y. 1998. Quantum effects in simulated water by the Feynman Hibbs approach. *J. Chem. Phys.* 108:10162–74
83. Hernandez de la Pena L, Kusalik PG. 2004. Quantum effects in light and heavy liquid water: a rigid-body centroid molecular dynamics study. *J. Chem. Phys.* 121:5992–6002
84. Poulsen JA, Nyman G, Rossky PJ. 2005. Static and dynamic quantum effects in molecular liquids: a linearized path integral description of water. *Proc. Natl. Acad. Sci. USA* 102:6709–14
85. Chen B, Ivanov I, Klein ML, Parrinello M. 2003. Hydrogen bonding in water. *Phys. Rev. Lett.* 91:215503
86. Li XZ, Walker B, Michaelides A. 2011. Quantum nature of the hydrogen bond. *Proc. Natl. Acad. Sci. USA* 108:6369–73

87. Markland TE, Berne BJ. 2012. Unraveling quantum mechanical effects in water using isotopic fractionation. *Proc. Natl. Acad. Sci. USA* 109:7988–91
88. Liu J, Miller WH, Paesanim F, Zhang W, Case DA. 2009. Quantum dynamical effects in liquid water: a semiclassical study on the diffusion and the infrared absorption spectrum. *J. Chem. Phys.* 131:164509
89. Hammes-Schiffer S, Tully JC. 1994. Proton transfer in solution: molecular dynamics with quantum transitions. *J. Chem. Phys.* 101:4657–67
90. Kim SY, Hammes-Schiffer S. 2003. Molecular dynamics with quantum transitions for proton transfer: quantum treatment of hydrogen and donor-acceptor motions. *J. Chem. Phys.* 119:4389–98
91. McRae RP, Schenter GK, Garrett BC, Svetlicic Z, Truhlar DG. 2001. Variational transition state theory evaluation of the rate constant for proton transfer in a polar solvent. *J. Chem. Phys.* 115:8460–80
92. Yamamoto T, Miller WH. 2005. Path integral evaluation of the quantum instanton rate constant for proton transfer in a polar solvent. *J. Chem. Phys.* 122:044106
93. Hanna G, Kapral R. 2005. Quantum-classical Liouville dynamics of nonadiabatic proton transfer. *J. Chem. Phys.* 122:244505
94. Nagel ZD, Meadows CW, Dong M, Bahnson BJ, Klinman JP. 2012. Active site hydrophobic residues impact hydrogen tunneling differently in a thermophilic alcohol dehydrogenase at optimal versus nonoptimal temperatures. *Biochemistry* 51:4147–56
95. Meyer MP, Tomchick DR, Klinman JP. 2008. Enzyme structure and dynamics affect hydrogen tunneling: the impact of a remote side chain (I553) in soybean lipoxygenase-1. *Proc. Natl. Acad. Sci. USA* 105:1146–51
96. Ananth N, Miller TF. 2012. Flux-correlation approach to characterizing reaction pathways in quantum systems: a study of condensed-phase proton-coupled electron transfer. *Mol. Phys.* 110:1009–15
97. Habershon S, Fanourgakis GS, Manolopoulos DE. 2008. Comparison of path integral molecular dynamics methods for the infrared absorption spectrum of liquid water. *J. Chem. Phys.* 129:074501
98. Witt A, Ivanov SD, Shiga M, Forbert H, Marx D. 2009. On the applicability of centroid and ring polymer path integral molecular dynamics for vibrational spectroscopy. *J. Chem. Phys.* 130:194510
99. Shi Q, Geva E. 2003. Semiclassical theory of vibrational energy relaxation in the condensed phase. *J. Phys. Chem. A* 107:9030–46
100. Shi Q, Geva E. 2003. Vibrational energy relaxation in liquid oxygen from a semiclassical molecular dynamics simulation. *J. Phys. Chem. A* 107:9070–78
101. Shi Q, Geva E. 2003. On the calculation of vibrational energy relaxation rate constants from centroid molecular dynamics simulations. *J. Chem. Phys.* 119:9030–46
102. Horikoshi A, Kinugawa K. 2005. Effective potential analytic continuation approach for real time quantum correlation functions involving nonlinear operators. *J. Chem. Phys.* 122:174104
103. Rahman A, Singwi KS, Sjolander A. 1962. Theory of slow neutron scattering by liquids. *Phys. Rev.* 126:986–96
104. Gubernatis JE, Jarrell M, Silver RN, Sivia DS. 1991. Quantum Monte Carlo simulations and maximum entropy: dynamics from imaginary-time data. *Phys. Rev. B* 44:6011–29
105. Gallicchio E, Berne BJ. 1994. The absorption spectrum of the solvated electron in fluid helium by maximum entropy inversion of imaginary time correlation functions from path integral Monte Carlo simulations. *J. Chem. Phys.* 101:9909–18
106. Gallicchio E, Berne BJ. 1996. On the calculation of dynamical properties of solvated electrons by maximum entropy analytic continuation of path integral Monte Carlo data. *J. Chem. Phys.* 105:7064–78
107. Jarrell M, Gubernatis JE. 1996. Bayesian inference and the analytic continuation of imaginary-time Monte Carlo data. *Phys. Rep.* 269:133–95
108. Krilov G, Sim E, Berne BJ. 2001. Quantum time correlation functions from complex time Monte Carlo simulations: a maximum entropy approach. *J. Chem. Phys.* 114:1075–88
109. Rabani E, Reichman DR, Krilov G, Berne BJ. 2002. The calculation of transport properties in quantum liquids using the maximum entropy numerical analytic continuation method: application to liquid *para*-hydrogen. *Proc. Natl. Acad. Sci. USA* 99:1129–33
110. Braams BJ, Miller TF, Manolopoulos DE. 2006. Sum rule constraints on Kubo-transformed correlation functions. *Chem. Phys. Lett.* 418:179–84
111. Marcus RA, Sutin N. 1985. Electron transfers in chemistry and biology. *Biochim. Biophys. Acta* 811:265–322

112. Kuharski RA, Bader JS, Chandler D, Sprik M, Klein ML, Impey RW. 1988. Molecular model for aqueous ferrous-ferric electron transfer. *J. Chem. Phys.* 89:3248–57
113. Egorova D, Domcke W. 2004. Quantum dynamical simulations of ultrafast photoinduced electron-transfer processes. *J. Photochem. Photobiol. A* 166:19–31
114. Egorova D, Thoss M, Domcke W, Wang HB. 2003. Modeling of ultrafast electron-transfer processes: validity of multilevel Redfield theory. *J. Chem. Phys.* 119:2761–73
115. Klauder JR. 1997. Coherent state quantization of constraint systems. *Ann. Phys.* 254:419–53
116. Meyer HD, Miller WH. 1979. A classical analog for electronic degrees of freedom in nonadiabatic collision processes. *J. Chem. Phys.* 70:3214–23
117. Tully JC. 1998. Mixed quantum-classical dynamics. *Faraday Discuss.* 110:407–19
118. Stock G, Thoss M. 1997. Semiclassical description of nonadiabatic quantum dynamics. *Phys. Rev. Lett.* 78:578–81
119. Ananth N, Miller TF. 2010. Exact quantum statistics for electronically nonadiabatic systems using continuous path variables. *J. Chem. Phys.* 133:234103
120. Nielsen S, Kapral R, Ciccotti G. 2001. Statistical mechanics of quantum-classical systems. *J. Chem. Phys.* 115:5805–15
121. Schmidt JR, Parandekar PV, Tully JC. 2008. Mixed quantum-classical equilibrium: surface hopping. *J. Chem. Phys.* 129:044104
122. Marcus RA. 1993. Electron transfer reactions in chemistry: theory and experiment. *Rev. Mod. Phys.* 65:599–610
123. Eastman P, Pande VS. 2010. OpenMM: a hardware-independent framework for molecular simulations. *Comput. Sci. Eng.* 12:34–39
124. Case DA, Cheatham TE, Darden T, Gohlke H, Luo R, et al. 2005. The Amber biomolecular simulation programs. *J. Comput. Chem.* 26:1668–88